Polímeros
ISSN 1678-5169 (Online)

https://doi.org/10.1590/0104-1428.20210102

ORIGINAL ARTICLE

Physical-mechanical behavior of nitrile rubber-synthetic mica nanocomposites

Janis Schutte Nunes[1]*, Edson Noriyuki Ito[2], Cléverson Fernandes Senra Gabriel[1,3], Thiago Castro Lopes[1] and Regina Célia Reis Nunes[1]

[1]Instituto de Macromoléculas – IMA, Universidade Federal do Rio de Janeiro – UFRJ, Rio de Janeiro, RJ, Brasil
[2]Centro de Tecnologia, Departamento de Engenharia de Materiais, Universidade Federal do Rio Grande do Norte – UFRN, Natal, RN, Brasil
[3]Laboratório de Tecnologia de Materiais Poliméricos – LAMAP, Instituto Nacional de Tecnologia – INT, Rio de Janeiro, RJ, Brasil
**janis_schutte@yahoo.com.br*

Abstract

Nitrile rubber (NBR) nanocomposites with different contents of synthetic Somasif ME-100 mica (sodium-fluorohectorite) were obtained by melt compounding using a Semi Efficient curing system. The effect of curing on the nanocomposties was evaluated through rheometric properties, crosslink density (CLD) and mechanical properties. The ME-100 mica dispersion in NBR was assessed by transmission electron microscopy (TEM), the Payne effect and thermodynamic properties (ΔS and ΔG). Both the curing parameters and CLD pointd out that the addition of ME-100 directly affects crosslinks formation. It could also be observed that the nanofiller dispersion state is complex, exhibiting exfoliated and agglomerated structures (TEM); besides, agglomerations rose linearly as the nanofiller was added (the Payne effect). Notwithstanding these findings, and on the basis of unfilled formulations, NBR20 nanocomposite showed improvement in mechanical properties (tensile and tear strengths) which suggests that ME-100 might be considered a semi-reinforcing filler.

Keywords: *crosslink density, fluoromica, mechanical properties, nitrile rubber, synthetic mica.*

How to cite: Nunes, J. S., Ito, E. N., Gabriel, C. F. S., Lopes, T. C., & Nunes, R. C. R. (2022). Physical-mechanical behavior of nitrile rubber-synthetic mica nanocomposites. *Polímeros: Ciência e Tecnologia*, *32*(2), e2022021. https://doi.org/10.1590/0104-1428.20210102

1. Introduction

The high polarity of nitrile rubber (NBR), a copolymer of butadiene and acrylonitrile, makes it highly resistant to oils and organic solvents, while having low gas permeability and temperature degradation higher than natural rubber. These features enable its use in automotive products, oil seals, fuel hoses, among others[1,2].

In order to provide technological application, depending on the application of the final product, the formulation of an elastomeric composition usually contain a filler, a curing system, processing and protecting agents such as antioxidants[3]. These components alter the compound viscosity with direct impact on processing as well as on the final product physical mechanical properties[4,5].

Carbon black and silica are the most widely used reinforcement fillers for elastomeric formulations, besides, other fillers, functionalized or not, have been widely employed as an alternative to the conventional systems[6]. A significant amount of research papers has been directed to the development and use of different fillers with dimensions in the nanometric scale, clays being highlighted[6-11].

Among the group of clays being employed as nanofillers of elastomeric compositions, the synthetic micas should be highlighted. Their main advantages, as compared to natural mica, are better control of variables such as purity and composition, besides the possibility of altering their structure for fitting in with the matrix into which they will be incorporated[12-20].

The synthetic mica marketed as Somasif ME-100 (sodium-fluorohectorite) is prepared from talc by introducing an alkaline metal in the interlamellar galleries[21]. Somasif ME-100, as well as montmorillonite, exhibits a layered silicate structure but differs from the latter by the absence of catalytically active Al ions as substitutes at the octahedral sites. A further difference is the partial replacement of silicate layers hydroxyl groups by fluorine[22].

Because of the high viscosity of the elastomeric matrix, the dispersion of any inorganic material is a challenging task, chiefly when it is related to a nanofiller. In order to reach the desired dispersion degree, various methods are proposed in the literature[6,7].

In the last seven years, few works have been published with Somasif ME-100 synthetic mica[23,24]. The amount of articles is even smaller when it comes to the use of Somasif ME-100 with polymers[15,25-34]. This fluoromic was little explored in NBR, which is a very important rubber for the industry, and only one article was found in the literature

that correlates Somasif ME-100 with NBR[16]. Justifying the work's importance and novelty.

This work shows the continuity of Linhares et al.[16] work where ME-100 synthetic mica nanocomposites with NBR were prepared by melt compounding. This method being chosen by the versatility as concerns temperature, roller shear rate, and show practical relevance. The content of the ME-100 synthetic mica in this work varied from 0 to 20 phr. The 20phr ME-100 nanocomposite showed improvement in mechanical properties which suggests that ME-100 might be considered a semi-reinforcing filler.

2. Materials and Methods

2.1 Materials

The received nitrile rubber had the following features: Mooney viscosity 48 ML1+4 (100°C) and acrylonitrile content 33%. The synthetic mica for the compositions was sodium fluorohectorite (Somasif ME-100), with cation exchange capacity of 100 meq/100 g and an intergallery distance of 0.95 nm[20] and in this work will be referred to as ME-100. The characterization of this synthetic mica has already been carried out by our working group and can be found in Linhares et al.[16]. According to the manufacturer (COOP ChemicalCo. Ltd, Japan), Somasif mica ME-100 have the general chemical composition $(Na)_{2x}(Mg)_{3-x}(Si_4O_{10})(F_yOH_{1-y})_2 \cdot nH_2O$, where $0.15 < x < 0.5$; $0.8 < y < 1.0$.

The information on the prepared formulations is listed in Table 1, and an unfilled composition (NBR0) stands for comparison with the properties of the nanocomposites.

2.2 Sample preparation

The preparation of the mixes was done in an open roller mill, at 50±5°C. At first mica was added to the rubber for 10 minutes at a roller shear rate of 24/40 aiming at favoring the distribution and dispersion of mica into NBR[13,16]. This procedure was carried out in all formulations in order to maintain a mixing pattern. After this period of time, the vulcanization system was incorporated into the formulation at a shear rate of 24/34 in accordance with the ASTM D3187 Method. The samples' vulcanization process was performed by compression molding at the temperature of 160°C. The period of time used for molding was the optimum curing time (t90), determined with the aid of the Rubber Process Analyzer (RPA) instrument.

2.3 Characterization

2.3.1 Curing characteristics

The curing characteristics for the prepared mixtures were obtained using the Rubber Process Analyzer (RPA 2000 from the Monsanto Company) instrument, in accordance with the ASTM D5289 Method under the following experimental conditions: 160°C (constant temperature), 30 minutes, deformation arc 1 degree and 1.7 Hz of frequency. The RPA instrument enables the determination of the following rheometric parameters: pre-curing time (ts 1); optimum curing time (t90) related to 90% cure; minimum torque (ML); maximum torque (MH); cure rate index (CRI) the formula of which is given by Equation 1[35].

$$CRI(\%) = 100/(t90 - ts1) \quad (1)$$

2.3.2 Payne effect

The dependence of the dynamic properties on the deformation amplitude for all of the compositions was studied by the Payne Effect as measured by the RPA 2000 instrument at 60 ºC, test frequency of 1 Hz and strain from 0.7 to 100%[36,37]. The same procedure was adopted before and after curing. According to Payne, such dependence is essentially determined by the level of agglomeration and deglomeration of the filler tridimensional network in the elastomeric matrix[37].

The Payne effect can be calculated by the difference between the complex moduli in the region of low strains and high strains, see Equation 2, based on a specific strain value, temperature and frequency being kept constant[36-40].

$$\Delta G^* = G_0^* - G_\infty^* \quad (2)$$

Where ΔG* will be treated as the absolute value of the Payne Effect; besides, in this work the value of G^*_0 will be considered at 10% deformation while the value of G^*_∞ will be considered at 100% deformation.

2.3.3 Crosslink density

The crosslink density was measured with the aid of two different methods, the RPA Method and the swelling method.

In the RPA method the crosslink density (CD) is determined with the aid of the rubber processing analyzer RPA 2000. To this end the elastic modulus (G') of the uncured compounds ($G'_{uncured}$) was determined at a frequency of 5 Hz, the elastic modulus of the cured compouds (G'_{cured})

Table 1. Formulation of the mixes.

Material (phr)[1]	NBR0	NBR5	NBR7	NBR10	NBR14	NBR20
NBR	100	100	100	100	100	100
ME-100	0	5	7	10	14	20
Zinc Oxide	3.0	3.0	3.0	3.0	3.0	3.0
Stearic acid	1.0	1.0	1.0	1.0	1.0	1.0
Sulfur	1.5	1.5	1.5	1.5	1.5	1.5
TMTD[2]	0.5	0.5	0.5	0.5	0.5	0.5
MBT[3]	1.0	1.0	1.0	1.0	1.0	1.0

[1]per hundred rubber. [2]tetramethylthiuram disulfide. [3]2-mercaptobenzothiazole.

was determined at a frequency of 0.5 Hz at the temperature of 60°C and 0.25° deformation[41-43].

On the basis of the obtained results it is possible to estimate the total crosslinks (X_{total}) content in the sample, as well as the two types of crosslinks of the vulcanized rubbers: the physical links ($X_{physical}$), related to the physical entanglements of the polymer chains; the chemical links ($X_{chemical}$), generated in the vulcanization process, crosslinks[42]. Equation 3, Equation 4 and Equation 5 are used for the calculations.

$$X_{total} = G'_{cured}\left(0.5HZ\right) / 2RT \quad (3)$$

$$X_{physical} = G'_{uncured}\left(5HZ\right) / 2RT \quad (4)$$

$$X_{chemical} = X_{total} - X_{physical} \quad (5)$$

Where R = gas constant (8.314 L·kPa·K^{-1}·mol^{-1}); T = absolute temperature (333.15 K). In order to discount the presence of filler, Equation 6, the Guth-Gold[42] Equation, was used.

$$G'_{filled} = G'_{unfilled}\left(1 + 2.5\varnothing + 14.1\varnothing^2\right) \quad (6)$$

Where, ø is the filler volume fraction (filler volume / total volume).

The crosslink density (ν) was also determined with the aid of the solvent swelling principle, in this case acetone at 27°C, for the Flory-Rehner[44,45] solvent swelling equilibrium Equation 7:

$$\nu = -\frac{\left[ln\left(1-V_r\right) + V_r + \chi V_r^2\right]}{\left[V_0\left(V_r^{1/3} - V_r/2\right)\right]} \quad (7)$$

Where: ν is the value for the crosslink density; χ corresponds to the NBR-solvent interaction parameter, (0.345 for acetone), V0 is the solvent molar volume (73.40 mL.mol^{-1} for acetone), the solubility parameter for NBR (acrylonitrile content 33%) is δ = 9.36 (cal/cm)^2 [44] and Vr is the volume fraction of rubber in the swollen vulcanizate calculated by Equation 8 which discounts, when applicable, the volume of filler used[45,46].

$$V_r = \frac{\left(M_1/\rho_2\right) - \left(M_f/\rho_f\right)}{\left(M_1/\rho_2\right) - \left(M_f/\rho_f\right) + \left[\left(M_2 - M_3\right)/\rho_1\right]} \quad (8)$$

Where M_1 is the sample mass before swelling; ρ_2 is the sample density; M_f is the filler mass in the sample; ρ_f is the filler density; M_2 is the swollen sample mass; M_3 is the dry sample mass after swelling and ρ_1 is the solvent density.

Samples were cut from vulcanized, square 20x20 mm 2 mm-thick plates, tested in duplicate and kept in a tightly closed, protected from light acetone-containing flask, for a period of 7 days at ambient temperature (27ºC).

2.3.4 Thermodynamic characteristics

The value of V_r obtained in Equation 8 enables the calculation of the thermodynamic parameters. Based on the assumption that the internal energy of the tested materials has not been altered by swelling, the Gibbs free energy (ΔG) and the entropy variation (ΔS) can be determined by the Flory–Huggins equation and the statistical theory of the rubber elasticity (Equation 9 and Equation 10)[19,47-52].

$$\Delta G = RT\left[ln\left(1-V_r\right) + V_r + \chi V_r^2\right] \quad (9)$$

$$\Delta G = -T\Delta S \quad (10)$$

The parameters of Equation 9 have the same meaning as those of Equation 7, R being the gas constant and T the absolute temperature.

2.3.5 X-Ray Diffraction (XRD)

X-Ray Diffraction (XRD) was used for the characterization and identification of Mica ME-100 and generated composites. The XRD analysis was performed in a Rigaku equipment, model MiniFlex, with 2θ scanning from 2 to 10°, CuK α radiation (λ =1.5418 Å), 30 kV and 15 mA. The interplanar distances of mica were determined by the Bragg Equation (Equation 11), based on results obtained by X-ray scattering at high angles of incidence (WAXS).

$$d = \frac{n\lambda}{2\sin\theta} \quad (11)$$

Where: d is the interplanar distance, n is the diffraction order; θ is the diffraction angle (Bragg angle), n= 1 and λ=1.54 Å.

2.3.6 Mechanical properties

Elongation at break, tensile strength, modulus and tear strength tests were performed with the aid of a EMIC, model DL3000 universal testing machine operating with a 1 kN load cell in accordance with the ASTM D412 and ASTM D624 Methods, respectively. Hardness was determined with the Shore A durometer in accordance with the ASTM D2240 Method.

2.3.7 Transmission Electron Microscopy (TEM)

The morphology of the nanocomposites was studied by transmission electron microscopy (TEM). Samples were sectioned in a Power Tome Ultramicrotome RMC model X by using a Diatome Diamond Knife type Cryo 45°, cutting temperature -70°C cooled with liquid nitrogen, cutting speed 0.3 mm/s and cutting thickness 30 nm. After separation of the samples, samples-containing grids were taken to a Phillips transmission electronic microscope (TEM) model CM120 at an operation tension of 120 kV.

3. Results and Discussions

3.1 Curing and rheological behavior of NBR/ME-100 nanocomposites

The rheological parameters of the developed formulations are listed in Table 2.

The minimum torque (ML) values, related to the viscosity of compositions prior to cure, were kept practically constant

Table 2. Curing and Rheological Behavior of NBR/ME-100 Nanocomposites.

Parameter	NBR0	NBR5	NBR7	NBR10	NBR14	NBR20
Minimum Torque (ML) (dN.m)	0.7	0.7	0.7	0.7	0.7	0.8
Maximum Torque (MH) (dN.m)	9.1	7.9	8.1	8.8	9.0	9.6
ΔM (MH - ML) (dN.m)	8.4	7.2	7.4	8.1	8.3	8.8
Scorch time (ts_1) (min)	0.4	0.5	0.5	0.5	0.5	0.5
Optimum cure time (t_{90}) (min)	4.9	2.9	3.3	5,1	4.9	4.9
Cure rate index (CRI) (min)	22	42	36	22	23	23

with the filler content. It was expected that at 20 phr ME-100 the increase in ML would be significant, however the ME-100 lamellar structure provided a rheological ease for accommodation of the filler in the polymer matrix, indicating that the nanofiller acted as a processing aid.

The maximum torque (MH) represents post-cure molecular rigidity of the composites and it was only at 20phr ME-100 (NBR20) that the MH value outperformed that of the unfilled composition (NBR0). Data reflected on the torque (ΔM) development, generally used to characterize filler reinforcement and formation of an elastomeric network confined within the interlayer spaces[48,52,53]. These results point out that the ME-100 offers a certain resistance to crosslink formation, reducing the amount of curing agents available for the reaction. This behavior was also observed by Kader and Nah[53] and by Pojanavaraphan et al.[50] when evaluating other nanocomposites.

As regards the vulcanization pre-time (ts_1) there are no differences among the tested compositions, however, as for the period for 90% cure (t_{90}), it was observed that for compositions with 5 and 7 phr filler, curing occurs more rapidly as compared to the remaining formulations (< t90), reflecting in this way on the increased cure rate index (> CRI). For the remaining studied compositions these parameters are similar to those of the unfilled composition. Values suggest that for amounts of mica higher than 7 phr the filler is slightly interfering on the curing system, corroborating the effects on the tested ΔM.

3.2 The Payne effect

For elastomers with load exceeding Tg the Payne effect refers to the dependence of strain on the dynamic viscoelastic properties, For a constant frequency, the complex modulus (G*) is reduced with the increase in strain from a linear plateau value towards a lower plateau of high strain amplitude, as demonstrated in Figure 1A (before cure) and Figure 1B (after cure).

The value of the complex modulus (G*) for the NBR5 and NBR7 compositions was lower than that of the unfilled composition, NBR0, indicating that at low concentrations mica seems to aid the rubber chains to slip easier therefore reducing the energy required for strain to occur.

The filler network is destroyed under high strain and as a result, the complex modulus (G*) is quickly lowered. In this way, the modulus reduction consequent to augmented strain is also due to the rubber macromolecules entanglement and the break of the filler-filler and rubber-filler interactions. The lesser the attenuation of the dynamic modulus, the lower is the network structure formed by the filler, and the lower is the Payne effect. This indicates that the filler is

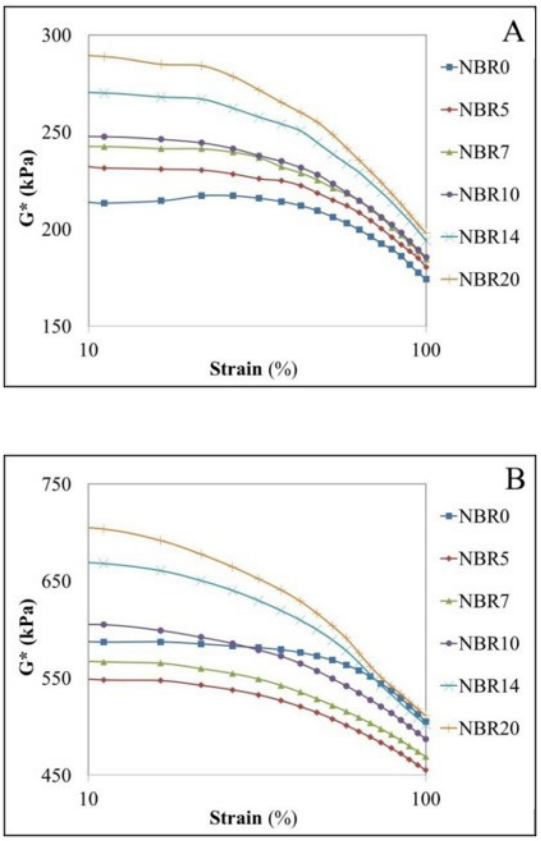

Figure 1. Variation of the Complex Modulus (G* - kPa) with strain (%) for unvulcanized (A) and vulcanized (B) NBR containing various amounts of ME-100 Mica.

better dispersed within the polymer matrix. As expected, for filled compositions, the increase in elastic modulus at low strains is attributed to the filler-filler interactions[26].

The values for the Payne effect calculated by the RPA Method for all of the compositions before and after cure are listed in Table 3.

The Payne effect analysis for pure gum before and after cure refers to the chain entanglement break that is more accentuated for the cured materials due to the higher viscosity of these solutions. As for the filled compositions, the influence of the rise in ME-100 content is observed by the increase in the Payne effect potentialized in the after cure compositions. These results illustrate the strong filler-filler interaction, which is equivalent to the agglomeration and deglomeration of the filler network.

3.3 Crosslink density

The results for crosslink density as determined by the RPA Method and solvent (acetone) swelling can be found in Table 4.

The RPA Method enables the calculation of two kinds of crosslinks: physical ($X_{physical}$) and chemical ($X_{chemical}$), and as a result the total crosslink density (X_{Total})[35,41,42,54]. Data acquisition is quick and does not require the use of solvents. The physical content means the initial crosslink density resulting from entanglements and other effects. Data (Table 4) indicate that the physical content was not modified by nanofillers to NBR. As for the chemical content, which results from the curing reaction, nanocomposites exhibited equivalent values and did not show any influence of the amount of filler, being lower than those for the unfilled compositions. The total crosslink density by RPA suggests that the slower curing reaction with the ME-100 content might probably due to cure retardation of ME-100 by adsorbing a part of the curing agents and blocking the movement of rubber chains as showed by the result of the chemical content. (Kader and Nah, 2004[53] and Pojanavaraphan, *et al.*, 2010[50]). An alternative for future work would be to increase the content of the curing system, as was successfully done by Kader and Nah[53]. The swelling values corroborate the results obtained for maximum torque (TM) and ΔM (Table 2) and crosslink density by RPA.

Results for crosslink density obtained by the swelling method (ν) and those for the volume fraction of rubber in the swollen vulcanizate (Vr), both determined by the Flory and Rhener theory for all the compositions can also be found in Table 4. Data obtained from the swelling test show reduced nanocomposites crosslink when compared with the unfilled compositions as a result from lower Vr values caused by the presence of ME-100 (Table 4). As compared with the values measured by RPA for the crosslink density, data for crosslink density by swelling are lower than those obtained by RPA, although more sensitive to the nanofiller behavior in the NBR.

The swelling behavior is in agreement with the data obtained by the rheometer and the value of the crosslink density by RPA suggest that the curing process has been restricted by ME-100 addition.

Table 3. The Payne effect of NBR/ME-100 nanocomposites before and after cure.

Composition	ΔG* before cure	ΔG* after cure
NBR0	39.3	82.1
NBR5	50.9	93.0
NBR7	58.2	97.7
NBR10	62.1	117.6
NBR14	76.0	166.1
NBR20	91.0	192.2

3.4 Thermodynamic characteristics

Thermodynamic effects, including entropy (ΔS) and Gibbs free energy (ΔG), that occur by swelling of the developed compositions were also determined and may provide the basis for understanding the nanofillers addition to NBR. The expansion of rubber in the presence of solvent will significantly modify the conformational entropy (ΔS) and the Gibbs free energy (ΔG)[19,47-52].

According to Table 5 the Gibbs free energy is negative for all samples. (ΔG) is correlated to the elastic behavior of the swollen compositions, influenced by the solvent, kind and ME-100 content in NBR.

It can be seen that in the presence of ME-100, ΔG falls (in absolute values) that is, the elasticity of the nanocomposites is lower than that of the pure gum in the swollen state. These results can be attributed to the low compatibility between NBR/ME-100, and are also responsible for the entropy loss as compared with the unfilled composition. The rubber molecules do not succeed in easily penetrating the galleries, hindering the process of ME-100 intercalation.

3.5 X-Ray Diffraction (XRD)

The Mica ME-100 diffractogram, which is represented in Figure 2, exhibited two peaks, one located at 7.05° and the other at 9.20°. These peaks correspond, respectively, to the interlamellar space (d001) of 1.25 nm and 0.96 nm (Table 6). According to Cattaneo et al.[55], the interlamellar space equal to 0.96 nm is related to the unhydrated silicate layer, while 1.25 nm corresponds to the hydrated form of the silicate layer.

The intercalation of polymeric chains in the silicate layers can be characterized by an increase in the interplanar spacing[56], however this was not observed. Based on the 2θ values of the XRD (Figure 2) and the stability of the interplanar distance (Table 6) of the formed composites, there is no evidence that there are NBR chains intercalated

Table 4. Crosslink density of the NBR composites with and without ME-100 Synthetic Mica.

Composition	RPA Method			Swelling Method	
	X_{Total}	$X_{physical}$	$X_{chemical}$	N	V_r
		(10^{-5}) mol/cm^3		(10^{-5}) mol/cm^3	cm^3
NBR0	9.7±0.1	2.7±0.1	7.0±0.1	70.5±0.9	0.306±0.001
NBR5	8.6±0.1	2.7±0.1	5.8±0.1	46.6±1.4	0.258±0.002
NBR7	8.6±0.1	2.7±0.1	5.8±0.1	52.7±0.6	0.271±0.009
NBR10	8.5±0.1	2.7±0.1	5.8±0.1	52.2±0.6	0.270±0.001
NBR14	8.5±0.1	2.7±0.1	5.8±0.1	51.9±0.2	0,269±0.001
NBR20	8.3±0.1	2.8±0.1	5.5±0.1	55.3±0.1	0.277±0.001

between the Mica layers. In addition, when we observe the increase in the intensity of the peaks of the composites formed, in relation to mica ME100, it is possible to affirm that the formed system predominantly presents agglomerations of filler, which increased with higher Mica ME100 content. This result is in agreement with that observed in the payne effect.

3.6 Mechanical properties

The mechanical properties of the nanocomposites are summarized in Table 7

Data of Table 7 might suggest ME-100 is acting as a semi-reinforcing filler in view of a 92% rise in tensile strength and 52% in elongation at break when data for the unfilled composition (NBR0) are compared with those for the highest filler-containing composition (NBR20), while values for hardness and minimum torque are unchanged. The mechanical results of the NBR7 sample, with the exception of the elongation, are within the experimental error. The elongation of NBR7 is an unexpected result and can be statistically compared to the value of this property with the unloaded composition (NBR0). However, it is the NBR7 composition that has the highest modulus at 100%, even higher than the composition with 20phr, and this result may be related to the low elongation value found. Therefore it is possible to state that the movement and accommodation of the rubber chains among the Mica lamellae was favored, this in turn increasing the chain fluidity, a fact that impacted the mechanical performance.

Concerning the tear strength, the compositions with higher-than 5 phr mica contents exhibited better performance as compared to the unfilled composition, and for the nanocomposite with 20 phr ME-100 a 42% increase was observed. As the cracks of the tear test propagate through the chains, they are restricted by the crosslinks which deform up to a certain point to hinder crack propagation. Since crosslinks values were very similar for all filled compositions and lower relative to the unfilled composition, it is possible to state that in this case the tear strength is directly related to the filler ability to dissipate crack propagation.

The lamellar nature, the plasticizing effect and a certain reluctance of the nanofiller for forming crosslinks can be understood in the light of the mechanical results related to molecular stiffness such as tensile strength at 50% elongation and 100% elongation, and hardness. These results did not exhibit significant increase with the filler content, corroborating the values for maximum torque determined by rheometry. These behaviors are interesting chiefly those for the 20 phr filler composition, since as compared with the unfilled composition it has better performance as regards tensile, elongation at break and tear strength values, hardness values being kept constant.

Table 5. Thermodynamic characteristics of the studied compositions.

Composition	ΔG (J.mol^{-1})	ΔS (J.mol^{-1}.K^{-1})
NBR0	-67.26	0.2241
NBR5	-43.34	0.1444
NBR7	-49.27	0.1641
NBR10	-48.91	0.1630
NBR14	-48.58	0.1618
NBR20	-51.97	0.1731

Table 6. Peak positions (2θ), interplanar spacing (d) of the Mica ME 100 peaks and their composites with NBRL, obtained by XRD.

Composition	2θ (Degrees)	Interplanar spacing, d(nm)
Mica ME100	7.05	1.25
	9.20	0.96
NBR0	-	-
NBR5	7.10	1.24
NBR7	7.15	1.23
NBR10	7.35	1.20
NBR14	7.05	1.25
NBR20	7.30	1.21

3.7 Transmission Electron Microscopy (TEM)

The TEM images of the NBR/ME-100 nanocomposites containing 5 phr (NBR5), 10 phr (NBR10) and 20 phr (NBR20) are illustrated in Figure 3, Figure 4 and Figure 5 respectively.

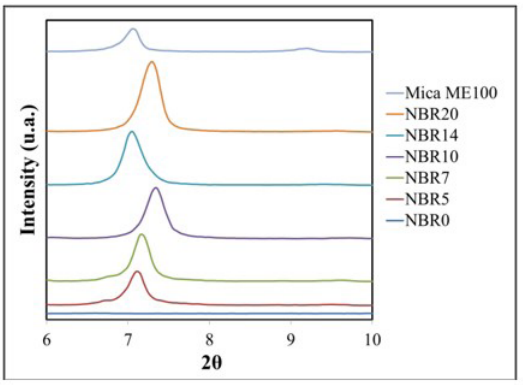

Figure 2. XRD pattern of NBR/Mica ME100 composites, unfilled NBR (NBR0), and Mica ME100 powder.

Table 7. Mechanical Properties.

Parameters	NBR0	NBR5	NBR7	NBR10	NBR14	NBR20
Elongation at break (%)	270±29	385±36	229±21	367±4	342±25	411±42
Tensile strength (MPa)	2.5±0,3	2.9±0,3	3.9±0.2	3.6±0.3	3.1±0.2	4.8±0.4
Modulus at 50% Elongation (MPa)	0.7±0.0	0.7±0.0	1.0±0.0	0.8±0.0	0.9±0.0	1.0±0.0
Modulus at 100% Elongation (MPa)	1.1±0.0	1.0±0.0	1.7±0.1	1.2±0.1	1.3±0.0	1.5±0.0
Tear strength (N/mm)	21±3	18±2	25±1	24±0	23±2	30±3
Hardness (Shore A)	47±1	43±1	42±1	44±1	45±1	47±1

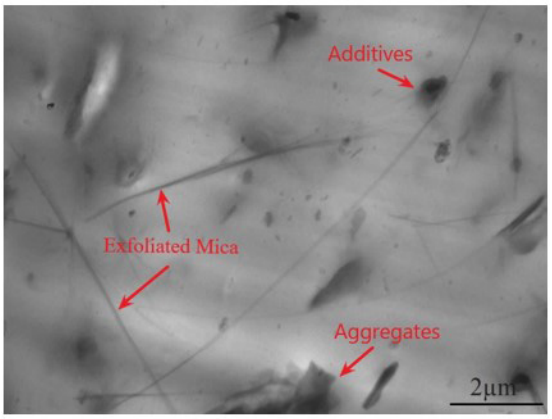

Figure 3. TEM images of the NBR5 nanocomposite at 8800x magnification.

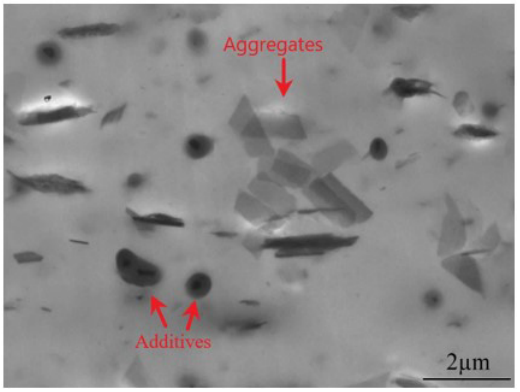

Figure 4. TEM images of the NBR10 nanocomposite at 8800x magnification.

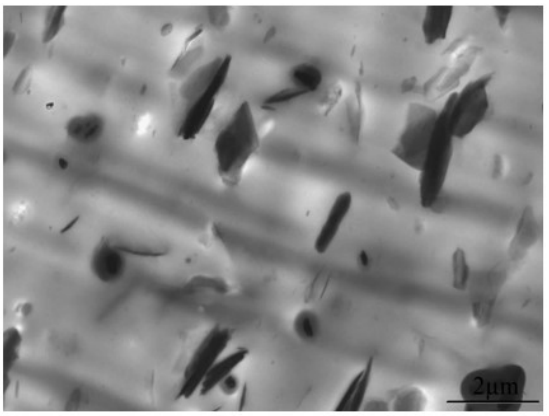

Figure 5. TEM images of the NBR20 nanocomposite at 8800x magnification.

As the filler content rises, evidences of exfoliated platelets and large aggregates are observed, corroborating the results for the Payne effect. Dark spots on the micrographs are related to the additives employed while the dark lines (Figure 3) show the nanofiller dispersion in the NBR matrix.

Taking into consideration that there is an optimum amount of ME-100 related to the intercalation/exfoliation phenomena, TEM results indicate that the rise in nanofiller content resulted in the morphology showing predominance of aggregates (Figure 4), fact that is in agreement with what was observed in the XRD, although without prejudice to the mechanical properties, as observed in this work. As for the case with the NBR composition containing 20 phr ME-100 (Figure 5) it is apparent that the layers and aggregates of the nanofiller created a morphology that resulted in improved mechanical properties[20], as shown in Table 7.

4. Conclusions

NBR nanocomposites of different contents of ME-100 synthetic mica were prepared by a mill mixing process and characterized.

The curing parameters indicated that the ME-100 offers a certain resistance to crosslink formation, reducing the amount of curing agents available for the reaction. This reluctance was ascertained by the analysis of the crosslink density, on the basis of the Flory and Rhener theory and RPA, both methods indicating the the crosslink density was always lower for the filled nanocomposites than for the unfilled nanocomposite. This phenomenon may have been caused by the formation of Mica ME100 clusters observed in both XRD and TEM results. These agglomerates may have made it difficult for sulfur to find the polymer chains and carry out the vulcanization reaction.

The values obtained for the Gibbs free energy can be attributed to the low compatibility between NBR and ME-100, and are also responsible for the entropy loss as compared to the unfilled composition. Besides, the dispersion state of ME-100 in NBR studied by the Payne effect indicated that the value of the modulus attenuation increased with increase in shear and with the filler content meaning low ME-100 dispersion in NBR. These results were corroborated by Transmission Electronic Microscopy (TEM) and XRD.

The TEM image and XRD of the 20 phr ME-100 nanocomposite demonstrated that the layers and aggregates of the nanofiller created a kind of morphology which might have been responsible for the improvement in mechanical properties, which suggests that ME-100 mica might be considered a semi-reinforcing filler.

Since NBR is an important, widely utilized rubber, the use of a light-colored nanofiller such as ME-100 can be of huge technological interest before the results obtained.

5. Author's Contribuition

• **Conceptualization –** Janis Schutte Nunes; Edson Noriyuki Ito; Cléverson Fernandes Senra Gabriel; Thiago Castro Lopes; Regina Célia Reis Nunes.
• **Data curation –** Janis Schutte Nunes; Cléverson Fernandes Senra Gabriel; Thiago Castro Lopes.
• **Formal analysis –** Janis Schutte Nunes; Cléverson Fernandes Senra Gabriel; Regina Célia Reis Nunes.
• **Investigation –** Janis Schutte Nunes; Edson Noriyuki Ito; Cléverson Fernandes Senra Gabriel; Thiago Castro Lopes; Regina Célia Reis Nunes.

• **Methodology –** Janis Schutte Nunes; Edson Noriyuki Ito; Cléverson Fernandes Senra Gabriel; Thiago Castro Lopes; Regina Célia Reis Nunes.
• **Project administration –** Regina Célia Reis Nunes.
• **Resources –** Edson Noriyuki Ito; Cléverson Fernandes Senra Gabriel; Regina Célia Reis Nunes.
• **Software –** Janis Schutte Nunes; Cléverson Fernandes Senra Gabriel; Thiago Castro Lopes.
• **Supervision –** Cléverson Fernandes Senra Gabriel; Regina Célia Reis Nunes.
• **Validation –** Regina Célia Reis Nunes; Cléverson Fernandes Senra Gabriel.
• **Visualization –** Regina Célia Reis Nunes; Edson Noriyuki Ito.
• **Writing – original draft –** Janis Schutte Nunes; Edson Noriyuki Ito; Cléverson Fernandes Senra Gabriel; Thiago Castro Lopes; Regina Célia Reis Nunes.
• **Writing – review & editing –** Janis Schutte Nunes; Edson Noriyuki Ito; Cléverson Fernandes Senra Gabriel; Thiago Castro Lopes; Regina Célia Reis Nunes.

6. Acknowledgements

Authors are indebted to CNPq, CAPES and FAPERJ for financial support and to Nitriflex S/A Indústria e Comércio for donation of the nitrile rubber, Co-Op Chemical Co. Ltda (Tokyo, Japan) for donation of the sodium fluorohectorite (Somasif ME-100) and Teadit Indústria e Comércio Ltda for donation of the additives utilized in the compositions.

7. References

1. Palaty, S., & Joseph, R. (2006). Low temperature curing of NBR for property improvement. *Journal of Elastomers and Plastics*, *38*(3), 199-209. http://dx.doi.org/10.1177/0095244306063479.
2. Schuster, H. R. (2019). *Dispersión de cargas y reforzamiento: ciencia y aplicación.* Buenos Aires: Sociedad Latinoamericana de Tecnologia del Caucho - SLTC.
3. Sisanth, K. S., Thomas, M. G., Abraham, J., & Thomas, S. (2017). *General introduction to rubber compounding.* In S. Thomas & H. J. Maria (Eds.), *Progress in rubber nanocomposites* (pp. 1-39). United Kingdom: Woodhead Publishing. http://dx.doi.org/10.1016/B978-0-08-100409-8.00001-2.
4. Sousa, A. M. F., Peres, A. C. C., Furtado, C. R. G., & Visconte, L. L. Y. (2017). Mixing process influence on thermal and rheological properties of NBR/SiO2 from rice husk ash. *Polímeros: Ciência e Tecnologia*, *27*(2), 93-99. http://dx.doi.org/10.1590/0104-1428.1959.
5. Morrill, J. P. (1968). *Nitrile Elastomers.* In G. G. Winspear (Ed.), *The vanderbilt rubber handbook* (pp. 169-188). USA: R. T. Vanderbilt Company, Inc.
6. Galimberti, M., Cipolletti, V., Musto, S., Cioppa, S., Peli, G., Mauro, M., Gaetano, G., Agnelli, S., Theonis, R., & Kumar, V. (2014). Recent advancements in rubber nanocomposites. *Rubber Chemistry and Technology*, *87*(3), 417-442. http://dx.doi.org/10.5254/rct.14.86919.
7. Das, A., Wang, D.-Y., Stockelhuber, K. W., Jurk, R., Fritzsche, J., Klüppel, M., & Heinrich, G. (2011). *Rubber–clay nanocomposites: some recent results.* In G. Heinrich (Ed.), *Advanced polymer science* (pp. 85-166) Germany: Springer Berlin Heidelberg.
8. Kumar, V., & Lee, D.-J. (2016). Studies of nanocomposites based on carbon nanomaterials and RTV silicone rubber. *Journal of Applied Polymer Science*, *134*(4), 44407.
9. Monfared, A., & Jalali-Arani, A. (2015). Morphology and rheology of (styrene-butadiene rubber/acrylonitrile-butadiene rubber) blends filled with organoclay: the effect of nanoparticle localization. *Applied Clay Science*, *108*, 1-11. http://dx.doi.org/10.1016/j.clay.2015.02.012.
10. Pavlidou, S., & Papaspyrides, C. D. (2008). A review on polymer–layered silicate nanocomposites. *Progress in Polymer Science*, *33*(12), 1119-1198. http://dx.doi.org/10.1016/j.progpolymsci.2008.07.008.
11. Wang, Y.-Q., Wu, Y.-P., Zhang, H.-F., Zhao, W., Wang, C.-X., & Zhang, L.-Q. (2005). Preparation, structure, and properties of a Novel Rectorite/Nitrile Butadiene Rubber (NBR) nanocomposites. *Polymer Journal*, *37*(3), 154-161. http://dx.doi.org/10.1295/polymj.37.154.
12. Carrado, K. A. (2000). Synthetic organo- and polymer–clays: preparation, characterization, and materials applications. *Applied Clay Science*, *17*(1-2), 1-23. http://dx.doi.org/10.1016/S0169-1317(00)00005-3.
13. Gabriel, C. F. S. (2018). *Desenvolvimento e caracterização de composições de NBR em fardo e em látex com mica Somasif ME100TM* (Dissertação de mestrado). Instituto de Macromoléculas Professora Eloisa Mano, Universidade Federal do Rio de Janeiro, Rio de Janeiro, Brasil.
14. Gatos, K. G., Thomann, R., & Karger-Kocsis, J. (2004). Characteristics of ethylene propylene diene monomer rubber/organoclay nanocomposites resulting from different processing conditions and formulations. *Polymer International*, *53*(8), 1191-1197. http://dx.doi.org/10.1002/pi.1556.
15. Honorato, L., Dias, M. L., Azuma, C., & Nunes, R. C. R. (2016). Rheological properties and curing features of natural rubber compositions filled with fluoromica ME 100. *Polímeros: Ciência e Tecnologia*, *26*(3), 249-253. http://dx.doi.org/10.1590/0104-1428.2352.
16. Linhares, F. N., Gabriel, C. F. S., Sousa, A. M. F., & Nunes, R. C. R. (2018). Mechanical and rheological properties of nitrile rubber/fluoromica composites. *Applied Clay Science*, *162*, 165-174. http://dx.doi.org/10.1016/j.clay.2018.06.004.
17. Psarras, G. C., Gatos, K. G., Karahaliou, P. K., Georga, S. N., Krontiras, C. A., & Karger-Kocsis, J. (2007). Relaxation phenomena in rubber/layered silicate nanocomposites. *Express Polymer Letters*, *1*(12), 837-845. http://dx.doi.org/10.3144/expresspolymlett.2007.116.
18. Varghese, S., & Karger-Kocsis, J. (2003). Natural rubber-based nanocomposites by latex compounding with layered silicates. *Polymer*, *44*(17), 4921-4927. http://dx.doi.org/10.1016/S0032-3861(03)00480-4.
19. Varghese, S., Karger-Kocsis, J., & Gatos, K. G. (2003). Melt compounded epoxidized natural rubber/layered silicate nanocomposites: structure-properties relationships. *Polymer*, *44*(14), 3977-3983. http://dx.doi.org/10.1016/S0032-3861(03)00358-6.
20. Varghese, S., Gatos, K. G., Apostolov, A. A., & Karger-Kocsis, J. (2004). Morphology and mechanical properties of layered silicate reinforced natural and polyurethane rubber blends produced by latex compounding. *Journal of Applied Polymer Science*, *92*(1), 543-551. http://dx.doi.org/10.1002/app.20036.
21. Tateyama, H., Tsunematsu, K., Kimura, K., Hirosue, H., Jinnai, K., & Furusawa, T. (2010). *US 5204078A*. Retrieved in 2021, December 2, from https://patentimages.storage.googleapis.com/93/21/18/e0caa019ef57dd/US5204078.pdf
22. Gelfer, M. Y., Burger, C., Nawani, P., Hsiao, B. S., Chu, B., Si, M., Rafailovich, M., Panek, G., Jeschke, G., Fadeev, A. Y., & Gilman, J. W. (2007). Lamellar nanostructure in "Somasif"-based organoclays. *Clays and Clay Minerals*, *55*(2), 140-150. http://dx.doi.org/10.1346/CCMN.2007.0550203.

23. Klabunde, S., Doerenkamp, C., Oliveira, M., Zeng, Z., & Eckert, H. (2021). Inorganic-organic hybrid materials based on the intercalation of radical cations: 2-(4-N-methylpyridinium)-4, 4, 5, 5-tetramethyl-4, 5-dihydro-1H-imidazol-1-oxyl-3-N-oxide in fluoromica clay. *Zeitschrift für Physikalische Chemie*, *236*(6-8), 961-978. http://dx.doi.org/10.1515/zpch-2021-3133.
24. Sugiura, M., Sueyoshi, M., Seike, R., Hayashi, T., & Okada, T. (2020). Hydrated silicate layer formation on mica-type crystals. *Langmuir*, *36*(18), 4933-4941. http://dx.doi.org/10.1021/acs.langmuir.0c00358. PMid:32330044.
25. Alosime, E. M., Edwards, G. A., & Martin, D. J. (2015). Structure-property relationships in copolyester elastomer-layered silicate nanocomposites. *Journal of Applied Polymer Science*, *132*(13), 41742. http://dx.doi.org/10.1002/app.41742.
26. Balcerzak, M., Pietralik, Z., Domka, L., Skrzypczak, A., & Kozak, M. (2015). Adsorption of dimeric surfactants in lamellar silicates. *Nuclear Instruments & Methods in Physics Research. Section B, Beam Interactions with Materials and Atoms*, *364*, 108-115. http://dx.doi.org/10.1016/j.nimb.2015.07.135.
27. Fukushima, Y., Yamada, T., Tamura, K., & Shibata, K. (2018). Dynamic of organic species in organo-clay/polypropyrene composite by quesi-elastic neutron scattering. *Applied Clay Science*, *155*, 15-19. http://dx.doi.org/10.1016/j.clay.2017.12.041.
28. Huth, M., Chen, C.-W., & Wagner, V. (2018). Measurement of Hansen solubility parameters for organophilic fluoromica and evaluation of potential solvents for exfoliation. *Applied Clay Science*, *155*, 120-125. http://dx.doi.org/10.1016/j.clay.2018.01.012.
29. Huth, M., Chen, C.-W., Köhling, J., & Wagner, V. (2018). Influence of Hansen solubility parameters on exfoliation of organophilic fluoromica. *Applied Clay Science*, *161*, 412-418. http://dx.doi.org/10.1016/j.clay.2018.04.036.
30. Kiersnowski, A., Chrissopoulou, K., Selter, P., Chlebosz, D., Hou, B., Lieberwirth, I., Honkimäki, V., Mezger, M., Anastasiadis, S. H., & Hansen, M. R. (2018). Formation of oriented polar crystals in bulk poly (vinylidene fluoride)/high-aspect-ratio organoclay nanocomposites. *Langmuir*, *34*(44), 13375-13386. http://dx.doi.org/10.1021/acs.langmuir.8b02412. PMid:30350703.
31. Leone, G., Giovanella, U., Galeotti, F., Barba, L., Arrighetti, G., Scavia, G., Rapallo, A., & Porzio, W. (2016). Conjugated dye-intercalated fluoromica hybrids displaying tunability of optical properties through packing variation. *Dyes and Pigments*, *124*, 53-62. http://dx.doi.org/10.1016/j.dyepig.2015.09.003.
32. Mohamadi, M., Garmabi, H., & Keshavarzi, F. (2016). An investigation of the effects of organomodified-fluoromica on mechanical and barrier properties of compatibilized high density polyethylene nanocomposite films. *Journal of Plastic Film & Sheeting*, *32*(1), 10-33. http://dx.doi.org/10.1177/8756087915569097.
33. Tee, N., Zhu, Y., Mortimer, G. M., Martin, D. J., & Minchin, R. F. (2015). Fluoromica nanoparticle cytotoxicity in macrophages decreases with size and extent of uptake. *International Journal of Nanomedicine*, *10*(1), 2363-2375. PMid:25848256.
34. Zhu, Y., Edwards, G. A., & Martin, D. J. (2015). Reduction of aspect ratio of fluoromica using high-energy milling. *Applied Clay Science*, *114*, 315-320. http://dx.doi.org/10.1016/j.clay.2015.06.020.
35. Dick, J. S., & Pawlowski, H. (1996). Applications for the curemeter maximum cure rate in rubber compound development process control and cure kinetic studies. *Polymer Testing*, *15*(3), 207-243. http://dx.doi.org/10.1016/0142-9418(95)00033-X.
36. Payne, A. R. (1962). The dynamic properties of carbon black-loaded natural rubber vulcanizates. Part I. *Journal of Applied Polymer Science*, *6*(19), 57-63. http://dx.doi.org/10.1002/app.1962.070061906.
37. Payne, A. R. (1962). The dynamic properties of carbon black loaded natural rubber vulcanizates. Part II. *Journal of Applied Polymer Science*, *6*(21), 368-372. http://dx.doi.org/10.1002/app.1962.070062115.
38. Niedermeier, W., Fröhlich, J., & Luginsland, H. D. (2002). Reinforcement mechanism in the rubber matrix by active fillers. *Kautschuk und Gummi, Kunststoffe*, *55*(7-8), 356-366.
39. Payne, A. R. (1963). Dynamic properties of heat-treated butyl vulcanizates. *Journal of Applied Polymer Science*, *7*(3), 873-885. http://dx.doi.org/10.1002/app.1963.070070307.
40. Payne, A. R., & Whittaker, R. E. (1971). Low strain dynamic properties of filled rubbers. *Rubber Chemistry and Technology*, *44*(2), 440-478. http://dx.doi.org/10.5254/1.3547375.
41. Chattaraj, P. P., Mukhopadhyay, R., & Tripathy, D. K. (1997). Effect of trans-polyoctenylene on crosslink structure of NBR and SBR using solid state ^{13}C NMR Spectroscopy and RPA 2000. *Rubber Chemistry and Technology*, *70*(1), 90-105. http://dx.doi.org/10.5254/1.3538421.
42. Lee, S., Pawlowski, H., & Coran, A. Y. (1994). Method for estimating the chemical crosslink densities of cured natural rubber and styrene-butadiene rubber. *Rubber Chemistry and Technology*, *67*(5), 854-864. http://dx.doi.org/10.5254/1.3538716.
43. Pechurai, W., Sahakaro, K., & Nakason, C. (2009). Influence of phenolic curative on crosslink density and other related properties of dynamically cured NBR/HDPE blends. *Journal of Applied Polymer Science*, *113*(2), 1232-1240. http://dx.doi.org/10.1002/app.30036.
44. Lapa, V. L. C., Oliveira, P. D., Visconte, L. L. Y., & Nunes, R. C. R. (2008). Investigation of NBR-cellulose II nanocomposites by rheometric and equilibrium swelling properties. *Polymer Bulletin*, *60*(2), 281-290. http://dx.doi.org/10.1007/s00289-007-0848-8.
45. Flory, P. J. (1953). *Principles of polymer chemistry*. USA: Cornell University Press.
46. Flory, P. J., & Rehner, J., Jr (1943). Statistical mechanics of crosslinked polymer networks I. Rubberlike elasticity. *The Journal of Chemical Physics*, *11*(11), 512-520. http://dx.doi.org/10.1063/1.1723791.
47. Hwang, W.-G., Wei, K.-H., & Wu, C.-M. (2005). Synergistic effect of compatibilizer in organo-modified layered silicate reinforced butadiene rubber nanocomposites. *Polymer Engineering and Science*, *46*(1), 80-88. http://dx.doi.org/10.1002/pen.20450.
48. López-Manchado, M. A., Herrero, B., & Arroyo, M. (2003). Preparation and characterization of organoclay nanocomposites based on natural rubber. *Polymer International*, *52*(7), 1070-1077. http://dx.doi.org/10.1002/pi.1161.
49. Mousa, A., & Karger-Kocsis, J. (2001). Rheological and thermodynamical behavior of styrene/butadiene rubber-organoclay nanocomposites. *Macromolecular Materials and Engineering*, *286*(4), 260-266. http://dx.doi.org/10.1002/1439-2054(20010401)286:4<260::AID-MAME260>3.0.CO;2-X.
50. Pojanavaraphan, T., Schiraldi, D. A., & Magaraphan, R. (2010). Mechanical, rheological, and swelling behavior of natural rubber/montmorillonite aerogels prepared by freeze-drying. *Applied Clay Science*, *50*(2), 271-279. http://dx.doi.org/10.1016/j.clay.2010.08.020.
51. Ghari, H. S., & Jalali-Arani, A. (2016). Nanocomposites based on natural rubber, organoclay and nano-calcium carbonate: study on the structure, cure behavior, static and dynamic-mechanical properties. *Applied Clay Science*, *119*(Part 2), 348-357. http://dx.doi.org/10.1016/j.clay.2015.11.001.
52. Tager, A. (1953). *Physical chemistry of polymers*. New York: Cornell University Press.
53. Kader, M. A., & Nah, C. (2004). Influence of clay on the vulcanization kinetics of fluoroelastomer nanocomposites. *Polymer*, *45*(7), 2237-2247. http://dx.doi.org/10.1016/j.polymer.2004.01.052.

54. Zhao, F., Shi, X., Chen, X., & Zhao, S. (2010). Interaction of vulcanization and reinforcement of CB on dynamic property of NBR characterized by RPA2000. *Journal of Applied Polymer Science*, *117*(2), 1168-1172. http://dx.doi.org/10.1002/app.31918.

55. Cattaneo, A. S., Bracco, S., Comotti, A., Galimberti, M., Sozzani, P., & Eckert, H. (2011). Structural characterization of pristine and modified fluoromica using multinuclear solid-state NMR. *The Journal of Physical Chemistry C*, *115*(25), 12517-12529. http://dx.doi.org/10.1021/jp2020676.

56. Khederlou, K., Bagheri, R., & Shojaei, A. (2014). A mathematical method for XRD pattern interpretation in clay containing nano composites. *Applied Surface Science*, *318*, 90-94. http://dx.doi.org/10.1016/j.apsusc.2014.01.044.

Received: Dec. 02, 2021
Revised: July 07, 2022
Accepted: July 21, 2022